ARTICLE

Synthesis and Characterization of Ethylene Glycol Substituted Poly(phenylene Vinylene) Derivatives

Chun-Chih Wang,[†] Hsinhan Tsai,[†] Hung-Hsin Shih,[†] Seaho Jeon,[†] Zhihua Xu,[‡] Darrick Williams,[§] Srinivas Iyer,[∥] Timothy C. Sanchez,[∥] Leeyih Wang,[⊥] Mircea Cotlet,*[,‡] and Hsing-Lin Wang*[,†]

Physical Chemistry and Applied Spectroscopy, Chemistry Division, Los Alamos National Laboratory, Mail Stop J567, Los Alamos, New Mexico 87545, Center for Functional Nanomaterials, Brookhaven National Laboratory, Mail Stop 735, Upton, New York 11973, Center of Integrated Nanotechnologies, Materials Physics and Applications Division, Los Alamos National Laboratory, Mail Stop K771, Los Alamos, New Mexico 87545, Bioscience Division, Los Alamos National Laboratory, Los Alamos, New Mexico 87545, and Center for Condensed Matter Sciences and Institute of Polymer Science and Technology, National Taiwan University, Taipei, Taiwan

ABSTRACT We report the synthesis of a series of water-soluble, fluorescent, conjugated polymers via the Gilch reaction with an overall yield greater than 40%. The yield for the Gilch reaction decreases with the increase in the length of the side chain (ethylene glycol repeat units), presumably due to the steric effects inhibiting the linking of monomeric units. The hydrophilic side chain enhances the solubility of the polymer in water and concomitantly leads to a side-chain-dependent conformation and solvent-dependent quantum efficiency. An increase in the ethylene glycol repeat units on the polymer side chain structure results in changes in chain packing; hence, the crystallinity evolves from semicrystalline to liquid crystalline to completely amorphous. An increase in the length of the side chain leads to changes in the polymer−solvent interaction as manifested in the photophysical properties of these polymers. These novel polymers exhibit two glass transition temperatures, which can be readily rationalized by differences in microstructure when casted from hydrophobic and hydrophilic solvents. Cyclic voltammograms of polymer **1d**−**3d** suggest two-electron transfer, as compared to **P1** which has one complete redox pair. The potential of having a nanoscaled domain structure and stabilizing two electrons on a polymer chain signifies the potential of these polymers in fabricating electronic and photovoltaic devices.

KEYWORDS: conjugated polymer • synthesis • optical properties • redox • photophysics

INTRODUCTION

Conjugated polymers emerge as exciting materials with real promises in the development of optical, electronic, and sensory devices (1−3). Among many conjugated polymers, polyphenylene vinylene (PPV) derivatives exhibit optical properties that can be tailored by modified chemical structures and by various processing parameters to which a low/high energy chain conformation is adapted. Of particular interest are water-soluble conjugated polymers because of their potential applications in the fabrication of light-emitting diodes (LED) by self-assembly methods (1−3) and in biosensing as highly sensitive fluorescent sensory materials in living bodies (4−7). The water-soluble PPVs are generally prepared by attaching hydrophilic charged units onto the polymer side chains. This includes anionic units such as carboxylate, phosphonate, and sulfonate groups and cationic units such as tertiary ammonium groups (8).

Because cationic conjugated polymers exhibit affinity toward anionic probes, they have been used in conjunction with DNA in bioassay platforms (6, 7) or with anionic pH sensitive dyes for chemosensing (9). Recently, Zhao et al. (10) have synthesized a series of conjugated poly(arylene ethynylene)s with high sensitivity toward molecular quenchers. We recently demonstrated the synthesis of cationic conjugated polymers with pH-dependent optical properties by protonating the amine groups on the polymer side chains (11). These polymers can sense subtle environmental (pH) changes and, therefore, act as highly sensitive chemosensors.

One category of water-soluble conjugated polymers that has been largely overlooked is the so-called "neutral" conjugated polymers, e.g., with no charge on the backbone. Various approaches were undertaken to induce solubility in water for this kind of polymers. For example, attachment of sugar molecules on the polymer side chain was shown to result in limited to moderate water solubility (12). Other popular approaches rendering solubility in water include the introduction of ethylene glycol (EG) as an alternating or block copolymer, with EG used as part of the polymer side chain structure along with a charged group (13−18). Winkler et

* To whom correspondence should be addressed. E-mail: hwang@lanl.gov (H.-L.W.); cotlet@bnl.gov (M.C.).
Received for review November 05, 2009 and accepted February 17, 2010
[†] Physical Chemistry and Applied Spectroscopy, Los Alamos National Laboratory.
[‡] Brookhaven National Laboratory.
[§] Center of Integrated Nanotechnology, Los Alamos National Laboratory.
[∥] Bioscience Division, Los Alamos National Laboratory.
[⊥] National Taiwan University.
DOI: 10.1021/am900766s

Published on Web 03/04/2010

al. (19, 20) synthesized PPV derivatives with side chains composed of a number of EG repeat units and a methoxy end group to fabricate LED devices. It should be mentioned that synthesis was carried mainly through a sulfonium precursor route and that the resultant polymer was not water soluble.

Here, we report the synthesis of a series of PPV derivatives with increasing number of EG repeating units and a tertiary imine end group to induce solubility both in organic and polar solvents. These as-synthesized conjugated polymers exhibit interesting physical and solvent dependent photophysics properties, including two glass transitions and two redox pairs, the latter presumably due to the inductive effect of ethylene glycol side chains.

EXPERIMENTAL SECTION

All reagents and solvents were purchased from Aldrich or Fisher and were used without further purification. The NMR spectra were collected on a Bruker-400 spectrometer using tetramethylsilane as internal reference. Cyclic voltammetry was performed at a concentration of ~10−3 M for polymer dissolved in dichloromethane and using *n*Bu4NPF6 (10^{-3} M) as an electrolyte. The working and counter electrodes were Pt and the reference electrode was Ag/AgCl. Cyclic voltammograms were acquired at a scan rate of 50 mV/s. UV−vis spectra were measured with a Varian Cary 500 UV−vis−near infrared (NIR-)spectrophotometer. Photoluminescence spectra were measured with a PTI Felix32 flourimeter. Photoluminescence quantum yield was measured using rhodamine 110 in water as a reference. Dynamic light scattering (DLS) measurements were performed on a Malvern Zetasizer Nano ZS instrument that uses the 632.5 nm line of a He:Ne laser. For instrument calibration, particle standards (polystyrene beads, 20 nm, Duke Scientific Co.) were used. The hydrodynamic volume of the polymer was estimated based on the Stokes−Einstein equation.

Photoluminescence decays were measured by the time-correlated single photon counting (TCSPC) method using 460 nm pulse laser excitation. The setup is described in (26) and it provides a response time of <100 ps. It is based on a frequency doubled Ti:Sapphire laser system (Newport Spectra Physics, 8.0 MHz repetition rate, 60 fs pulse width) and an inverted confocal fluorescence microscope (Olympus IX81) equipped with an oil immersion lens (Olympus IX81, Japan, 1.4 NA 100×). Fluorescence was detected at magic angle by a single photon counting avalanche photodiode (SPAD, MPD, Picoquant GmbH) and using a combination of dichroic mirror (Omega, 455DRLP) and band-pass filter (Omega 535/50) to ensure removal of the laser excitation. The signal from the SPAD was registered by a time-correlated single photon counting module (Picoharp 300, Picoquant GmbH). Decay histograms were collected with a time resolution of 4 ps per channel and analyzed by reiterative convolution of the instrumental response function (<100 ps) with an exponential model function using the FluoFit software (Picoquant GmbH). Matrix assisted desorption laser ionization mass spectrometry (MALDI-TOF MS) was performed on a 4800 Plus MALDI-TOFTOF system (Applied Biosystems, Framingham, MA) in positive ion, reflector mode. 2,5 Dihydroxybenzoic acid (DHB) was used as the matrix and prepared at a 1 mg/mL concentration in water. This solution was mixed 1:1 with the sample and spotted on a MALDI plate for analysis.

Synthesis of [2-(2-{4-[2-(2-Diethylamino-ethoxy)-ethoxy]-phenoxy}-ethoxy)-ethyl]-diethyl-amine (1b). A three-neck flask (250 mL) containing 2-[4-(2-hydroxy-ethoxy)-phenoxy]-ethanol (3 g, 15 mmol) and sodium hydride (1.08 g, 45 mmol) was evacuated and purged with nitrogen gas three times. Freshly distilled dry DMF (100 mL) was added to the flask via syringe and was stirred at 0 °C for 30 min, followed by the addition of 2-chlorotriethylamine hydrochloride (7.88 g, 45 mmol) via powder addition funnel. The mixture was heated with stirring at 80 °C for 3 h and was then cooled and diluted with ethyl acetate and water. The residue was extracted with ethyl acetate three times. The combined organic fractions were washed with sodium hydroxide (10%), water, and brine. The solution was then dried over MgSO4, filtered, and stripped of the solvent by rotary evaporation to yield a pale-yellow oil product (5.46 g, yield: 92%). ^{1}H NMR (400 MHz, $CDCl_3$): δ 6.81 (s, 4H), 4.03 (t, 4H), 3.76 (t, 4H), 3.61 (t, 4H), 2.67 (t, 4H), 2.56 (q, 8H), 1.01 (t, 12H). ^{13}C NMR (100 MHz, $CDCl_3$): δ 153.13, 115.58, 69.84, 69.69, 68.08, 52.22, 47.64, 11.58. MALDI-TOF mass spectrum calcd for $C_{22}H_{40}N_2O_4H^+$ [M + H$^+$]: 397.56. Found: 397.16.

Synthesis of [2-(2-{2,5-Bis-chloromethyl-4-[2-(2-diethylamino-ethoxy)-ethoxy]-phenoxy}-ethoxy)-ethyl]-diethyl-amine (1c). To a 40 mL of 37% formaldehyde aqueous solution was added concentrated HCl (30 mL) at 0 °C. The solution was saturated with HCl gas for 20 min before the addition of a suspension of **1b** (4 g, 10.08 mmol) in 10 mL of dioxane. The resulting mixture was allowed to stir at room temperature for 15 h. Once the reaction was complete, the solvents were removed by vacuum. The residue was then added into 50 mL of methanol, stirred for 20 min, filtered, and then repeatedly (three times) washed with ethyl acetate. The final white powder was dried under vacuum and used directly for the subsequent reaction without further purification (4 g, yield: 70%). ^{1}H NMR (400 MHz, $CDCl_3$): δ 6.95 (s, 2H), 4.63 (s, 4H), 4.16 (br. 4H), 4.10 (br, 4H), 3.87 (br, 4H), 3.24 (br, 4H), 3.18 (m, 8H), 1.39 (m, 12H). ^{13}C NMR (100 MHz, D_2O): δ 152.48, 131.74, 116.63, 72.83, 71.04, 66.70, 61.12, 53.36, 49.99, 10.46. MALDI-TOF mass spectrum calcd for $C_{24}H_{42}N_2Cl_2O_4$ [M]: 493.51. Found: 493.19.

Synthesis of Poly{[2-(2-{4-[2-(2-diethylamino-ethoxy)-ethoxy]-2-methyl-5-propenyl-phenoxy}-ethoxy)-ethyl]-diethyl-amine} (1d). A three-neck flask (250 mL) containing **1c** (2 g, 3.5 mmol) was evacuated and purged with nitrogen gas three times. Anhydrous THF (120 mL) was added to the flask via syringe and followed by the addition of *t*-BuOK (4 g, 35 mmol) in THF (40 mL) via addition funnel. The mixture was allowed to stir at room temperature for 24 h and poured into water (20 mL) to afford an orange solution. The orange solution was filtered and the solvent was evaporated in vacuum. The residue was extracted with CH_2Cl_2 three times. The combined organic fractions were dried over MgSO4, filtered, and stripped of the solvent by rotary evaporation to yield a red product. The red powder was washed with the mixed solvent of MeOH/H_2O (1:9) and dried under vacuum to afford orange-red product (1.05 g, yield: 71%). ^{1}H NMR (400 MHz, $CDCl_3$): δ 7.45 (br, 2H), 7.18 (br, 2H), 4.24 (br, 4H), 3.89 (br, 4H), 3.66 (br, 4H), 2.68 (br, 4H), 2.54 (m, 8H), 0.99 (m, 12H).

Synthesis of 2-(2-{4-[2-(2-Hydroxy-ethoxy)-ethoxy]-phenoxy}-ethoxy)-ethanol (2a). A two-neck flask (250 mL) containing 1,4-dihydroquinone (4 g, 36.4 mmol) and potassium carbonate (40 g, 291.2 mol) was evacuated and purged with nitrogen gas three times. Freshly distilled dry DMF (150 mL) was added to the flask via syringe and was stirred at room temperature for 30 min, followed by the addition of 2-(2-chloroethoxy)ethanol (18.1 g, 145.6 mmol). The mixture was heated with stirring at 80 °C for 7 days. After cooling to room temperature, the reaction was filtered and the residue was washed with DMF. The solvent was removed in vacuum, and the residue was extracted with CH_2Cl_2 and water three times. The combined organic fractions were dried ($MgSO_4$) and concentrated in vacuum. Recrystallization of the residue from CH_2Cl_2−hexane (1:2.5) afforded a white product (5.58 g, yield: 50%). ^{1}H NMR (400 MHz, $CDCl_3$): δ 6.82 (s, 4H), 4.05 (d, 4H), 3.81 (d, 4H), 3.73 (d, 4H), 3.63 (d, 4H), 2.47 (br, 2H). ^{13}C NMR

(100 MHz, $CDCl_3$): δ 153.05, 115.61, 72.60, 69.77, 68.03, 61.75. MALDI-TOF mass spectrum calcd for $C_{14}H_{22}O_6$ [M]: 286.32. Found: 286.08.

Synthesis of (2-{2-[2-(4-{2-[2-(2-Diethylamino-ethoxy)-ethoxy]-ethoxy}-phenoxy)-ethoxy]-ethoxy}-ethyl)-diethyl-amine (2b). A three-neck flask (250 mL) containing **2a** (4.3 g, 15.13 mmol) and sodium hydride (1.86 g, 77.5 mmol) was evacuated and purged with nitrogen gas three times. Freshly distilled dry DMF (120 mL) was added to the flask via syringe and was stirred at 0 °C for 30 min, followed by the addition of 2-chlorotriethylamine hydrochloride (7.88 g, 45 mmol) via powder addition funnel. The mixture was heated with stirring at 80 °C for 3 h and was then cooled and diluted with ethyl acetate and water. The residue was extracted with ethyl acetate three times. The combined organic fractions were washed with sodium hydroxide (10%), water, and brine. The solution was then dried over MgSO4, filtered, and stripped of the solvent by rotary evaporation to yield a yellow liquid (6.37 g, yield: 87%). ^{1}H NMR (400 MHz, $CDCl_3$): δ 6.75 (s, 4H), 3.97 (d, 4H), 3.74 (d, 4H), 3.61 (d, 4H), 3.55 (d, 4H), 2.46 (q, 8H), 0.92 (t, 12H). ^{13}C NMR (100 MHz, $CDCl_3$): δ 153.08, 115.55, 72.62, 70.28, 69.71, 69.65, 67.84, 52.02, 47.41, 11.52. MALDI-TOF mass spectrum calcd for $C_{26}H_{48}N_2O_6H^+$ [M + H^+]: 485.67. Found: 485.20.

Synthesis of (2-{2-[2-(2,5-Bis-chloromethyl-4-{2-[2-(2-diethylamino-ethoxy)-ethoxy]-ethoxy}-phenoxy)-ethoxy]-ethoxy}-ethyl)-diethyl-amine (2c). To a 40 mL of 37% formaldehyde aqueous solution was added concentrated HCl (30 mL) at 0 °C. The solution was saturated with HCl gas for 20 min before the addition of a suspension of **2b** (4 g, 8.2 mmol) in 10 mL of dioxane. The resulting mixture was allowed to stir at room temperature for 15 h. Once the reaction was complete, the solvents were removed by vacuum. The final oil product was dried under vacuum and used directly for the subsequent reaction without further purification (3.3 g, yield: 62%). ^{1}H NMR (400 MHz, D_2O): δ 7.08 (s, 2H), 4.66 (s, 4H), 4.21 (br, 4H), 3.90 (br, 4H), 3.76−3.6 (m, 12H), 3.45 (br, 4H), 3.20 (m, 8H), 1.26 (m, 12H). ^{13}C NMR (100 MHz, D_2O): δ 152.74, 131.95, 116.80, 72.49, 72.24, 72.07, 66.46, 61.51, 57.45, 53.71, 49.97, 10.53. MALDI-TOF mass spectrum calcd for $C_{28}H_{50}Cl_2N_2O_6$ [M]: 581.61. Found: 581.88.

Synthesis of Poly{(2-{2-[2-(4-{2-[2-(2-Diethylamino-ethoxy)-ethoxy]-ethoxy}-5-methyl-2-propenyl-phenoxy)-ethoxy]-ethoxy}-ethyl)-diethyl-amine} (2d). A three-neck flask (250 mL) containing **2c** (2 g, 3.0 mmol) was evacuated and purged with nitrogen gas three times. Anhydrous THF (120 mL) was added to the flask via syringe and followed by the addition of *t*-BuOK (4 g, 35 mmol) in THF (40 mL) via addition funnel. The mixture was allowed to stir at room temperature for 24 h and poured into water (20 mL) to afford an orange solution. The orange solution was filtered and the solvent was evaporated in vacuum. The residue was extracted with CH_2Cl_2 three times. The combined organic fractions were dried over $MgSO_4$, filtered, and stripped of the solvent by rotary evaporation to yield a red product (0.85 g, yield: 56%). ^{1}H NMR (400 MHz, $CDCl_3$): δ 6.99 (br, 2H) 6.89 (br, 2H), 4.37 (br, 2H), 4.07 (br, 4H), 3.75 (br, H), 3.65−3.47 (br, 12H), 2.61 (br, 4H), 2.43 (m, 8H), 0.95 (m, 12H).

Synthesis of 2-{2-[2-(4-{2-[2-(2-Hydroxy-ethoxy)-ethoxy]-ethoxy}-phenoxy)-ethoxy]-ethoxy}-ethanol (3a). A two-neck flask (250 mL) containing 1,4-dihydroquinone (4 g, 36.4 mmol) and potassium *t*-butoxide (8.9 g, 80 mol) was evacuated and purged with nitrogen gas three times. Freshly distilled dry *t*-butyl alcohol (70 mL) was added to the flask via syringe and was refluxed for 2 h, followed by the addition of 2-[2-(2-chloroethoxy)ethoxy]ethanol (13.5 g, 80 mmol) and refluxing was maintained for 3 days. After cooling to room temperature, the reaction mixture was filtered and the solid residue was washed with CH_2Cl_2. The solvent was removed in vacuum and the residue was extracted with CH_2Cl_2 and water. The combined organic fractions were dried ($MgSO_4$) and concentrated in vacuum. The residue was purified on a silica gel column using methanol−ethyl acetate (5:95) as eluent to afford a white product (6.5 g, yield 48%). ^{1}H NMR (400 MHz, $CDCl_3$): δ 6.69 (s, 4H), 3.89 (d, 4H), 3.65 (d, 4H), 3.54 (s, 8H), 3.50 (d, 4H), 3.41 (d, 6H). ^{13}C NMR (100 MHz, $CDCl_3$): δ 152.44, 114.96, 72.04, 70.11, 69.95, 69.98, 67.34, 60.89. MALDI-TOF mass spectrum calcd for $C_{18}H_{30}O_8$ [M]: 374.43. Found: 374.17.

Synthesis of {2-[2-(2-{2-[4-(2-{2-[2-(2-Diethylamino-ethoxy)-ethoxy]-ethoxy}-ethoxy)-phenoxy]-ethoxy}-ethoxy)-ethoxy]-ethyl}-diethyl-amine (3b). A three-neck flask (250 mL) containing **3a** (5.65 g, 15.1 mmol) and sodium hydride (1.86 g, 77.5 mmol) was evacuated and purged with nitrogen gas three times. Freshly distilled dry DMF (120 mL) was added to the flask via syringe and was stirred at 0 °C for 30 min, followed by the addition of 2-chlorotriethylamine hydrochloride (7.88 g, 45 mmol) via powder addition funnel. The mixture was heated with stirring at 80 °C for 3 h and was then cooled and diluted with ethyl acetate and water. The residue was extracted with ethyl acetate three times. The combined organic fractions were washed with sodium hydroxide (10%), water, and brine. The solution was then dried over $MgSO_4$, filtered, and stripped of the solvent by rotary evaporation to yield a yellow liquid (6.9 g, yield: 80%). ^{1}H NMR (400 MHz, $CDCl_3$): δ 6.82 (s, 4H), 4.05 (t, 4H), 3.80 (t, 4H), 3.68−3.60 (m, 16H), 3.53 (t, 4H), 2.63 (t, 4H), 2.53 (q, 8H), 0.99 (t, 12H). ^{13}C NMR (100 MHz, $CDCl_3$): δ 152.85, 115.37, 70.64, 70.44, 70.23, 69.66, 69.60, 67.79, 62.11, 52.00, 47.37, 11.58. MALDI-TOF mass spectrum calcd for $C_{230}H_{56}N_2O_8H^+$ [M + H^+]: 573.77. Found: 573.30.

Synthesis of {2-[2-(2-{2-[2,5-Bis-chloromethyl-4-(2-{2-[2-(2-diethylamino-ethoxy)-ethoxy]-ethoxy}-ethoxy)-phenoxy]-ethoxy}-ethoxy)-ethoxy]-ethyl}-diethyl-amine (3c). To a 40 mL of 37% formaldehyde aqueous solution was added concentrated HCl (30 mL) at 0 °C. The solution was saturated with HCl gas for 20 min before the addition of a suspension of **3b** (4 g, 7.0 mmol) in 10 mL of dioxane. The resulting mixture was allowed to stir at room temperature for 15 h. Once the reaction was complete, the solvents were removed by vacuum. The final oil product was dried under vacuum and used directly for the subsequent reaction without further purification (3.8 g, yield: 73%). ^{1}H NMR (400 MHz, D_2O): δ 7.04 (s, 2H), 4.74 (s, 4H), 4.61 (s, 4H), 4.15 (br, 4H), 3.86 (br, 4H), 3.75−3.6 (m, 16H), 3.26 (br, 4H), 3.13 (m, 8H), 1.19 (t, 12H). ^{13}C NMR (100 MHz, D_2O): 153.08, 132.34, 117.53, 84.61, 72.29, 72.14, 71.87, 71.36, 66.83, 61.89, 53.99, 50.04, 10.53. MALDI-TOF mass spectrum calcd for $C_{32}H_{58}Cl_2N_2O_8H^+$ [M + H^+]: 670.72. Found: 670.45.

Synthesis of Poly({2-[2-(2-{2-[4-(2-{2-[2-(2-Diethylamino-ethoxy)-ethoxy]-ethoxy}-ethoxy)-2-methyl-5-propenyl-phenoxy]-ethoxy}-ethoxy)-ethoxy]-ethyl}-diethyl-amine) (3d). A three-neck flask (250 mL) containing **3c** (2 g, 2.7 mmol) was evacuated and purged with nitrogen gas three times. Anhydrous THF (120 mL) was added to the flask via syringe and followed by the addition of *t*-BuOK (4 g, 35 mmol) in THF (40 mL) via addition funnel. The mixture was allowed to stir at room temperature for 24 h and poured into water (20 mL) to afford an orange solution. The orange solution was filtered, and the solvent was evaporated in vacuum. The residue was extracted with CH_2Cl_2 three times. The combined organic fractions were dried over MgSO4, filtered, and stripped off the solvent by rotary evaporation to yield a red product (0.78 g, yield: 48%). ^{1}H NMR (400 MHz, $CDCl_3$): δ 6.98 (br, 2H), 6.73 (br, 2H), 4.15 (br, 4H), 3.86 (br, 4H), 3.64−3.56 (m, 20H), 2.68 (m, 4H), 2.54 (m, 8H), 1.02 (t, 12H).

RESULTS AND DISCUSSIONS

Synthesis. Monomers **1c**−**3c** were prepared in a two-step reaction according to Scheme 1. Compounds **1a**−**3a** were prepared from 1,4-dihydroquinone according to the

Scheme 1. Synthetic Scheme of Polymers 1d−3d[a]

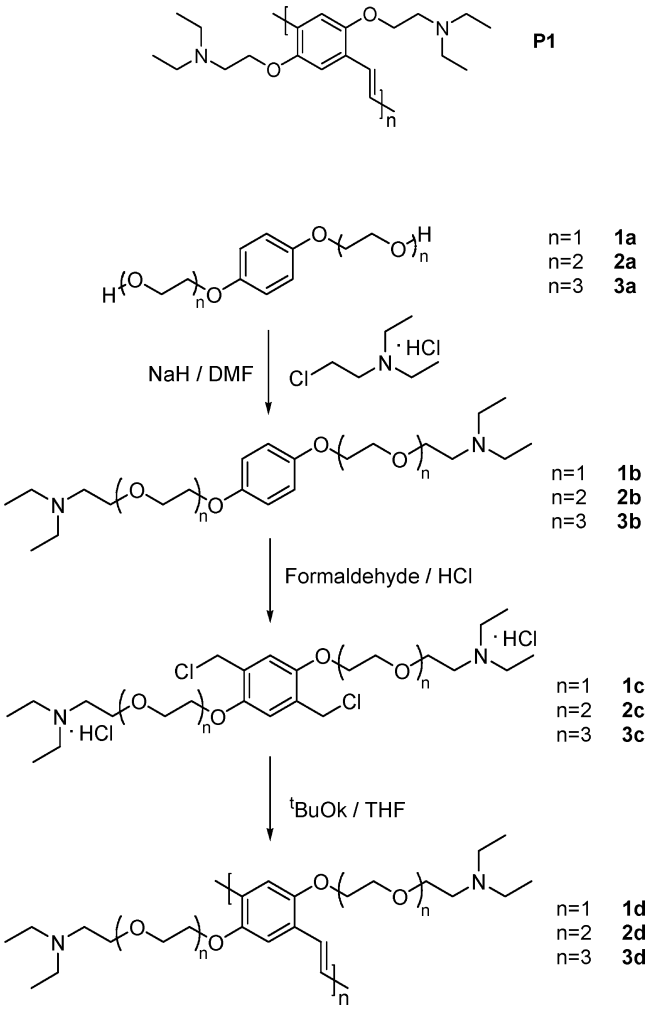

[a] Also shown is the chemical structure of polymer P1.

literature procedures (21). The reaction of **1a−3a** with 2-chlorotriethylamine hydrochloride in the presence of sodium hydride in DMF led to products **1b−3b**, which undergo chloromethylation with formaldehyde and hydrogen chloride to give white colored products **1c−3c**. The monomers **1c−3c** were used directly for the next step without further purification. **1c−3c** were polymerized in the potassium *tert*-butoxide (*t*-BuOK)−THF system to give the polymers **1d−3d**, in 71, 56 and 48% yields, respectively. The resulting bright red powder could be dissolved in common solvents, indicating that the ethylene oxide side chains were employed to allow for excellent solubility in organic solvents. In our previous study (11), the poly{2,5-bis[3-(*N*,*N*-diethylamino)-1-oxapropyl]-1,4-phenylenevinylene} (**P1** in Scheme 1) was soluble only in $CHCl_3$. Polymers **1d** and **2d** showed good solubility in common organic solvents such as chloroform, tetrahydrofuran, toluene, and CH_3OH, but they were barely soluble in H_2O. Polymer **3d**, however, is water-soluble, indicating enhanced polarity due to the ethoxy side chains. Polymers **1d−3d** were characterized by ^{1}H NMR and dynamic light scattering (DLS). ^{1}H NMR spectra of **1b**, **1c**, and **1d** are shown in Figure 1. The ^{1}H NMR spectrum of **1b** showed five peaks at 3.91 (t), 3.68 (t), 3.47 (t), 2.55 (t), and 2.43 (q) ppm for the methyl group, respectively. ^{1}H NMR of **1d** showed one broad peak at 7.4 ppm for trans vinyl protons, and the phenyl protons appeared at around 7.2 ppm in the spectrum. The ethoxy groups ($-CH_2CH_2O-$) were located at 4.3−2.7 ppm. The ethyl groups adjacent to nitrogen (CH_3CH_2N-) were observed as two peaks at 2.7 and 1.1 ppm, respectively. The average molecular weight of polymers **1d**, **2d**, **3d**, as determined by dynamic light scattering (DLS), is 15.8, 35.9, and 32.5 kDa, respectively (see Table 2).

Solubility. The as-synthesized polymers **P1**, **1d**, **2d**, and **3d** exhibit solubility which clearly relates to their molecular structure, in particular increased hydrophilicity for polymers with longer EG repeat units (see discussion below and Table 1). With increasing number of EG repeat units, these as-synthesized polymers become soluble in polar solvents. **P1** has limited solubility in organic solvents such as dichloromethane (DCM) (1 mg/mL), it is barely soluble in toluene (<0.1 mg/mL), and it is insoluble in polar solvents such as methanol and water. The limited solubility of **P1** is most likely due to a smaller side chain, which favors strong stacking interactions between phenylene vinylene backbone structures. There is a clear contrast between polymers with and without additional EG repeat units. Polymers **1d**, **2d**, and **3d** have additional EG repeat units on the side chains, and they are soluble in methanol, THF, ethylacetate (EA), DCM, and toluene. They only differ with respect to their solubility in water: polymer **1d** is barely soluble in water (pH = 7.0), **2d** has moderate solubility (3 mg/mL), and polymer **3d** is very soluble in water (>10 mg/mL).

Thermal Stability. Thermal properties of polymers **P1**, **1d**, **2d**, and **3d** were characterized by thermo gravimetric analysis (TGA) and differential scanning calorimetry (DSC). TGA and DSC data are summarized in Figure 2. All four polymers show decomposition temperatures (T_D) in the range 100−300 °C (see TGA curves in Figure 2a−d). Polymer **P1** is the most thermally stable ($T_D \sim 243$ °C, Figure 2a). Polymers **1d**, **2d**, and **3d** are not as thermally stable as **P1**, displaying some weight loss (5−15 wt %) at temperatures below 250 °C (see Figures 2a−d and Table 2) which is likely caused by a combination of water residue and a breakdown of the ethylene glycol molecules, with the latter known to decompose at around 160 °C (22). At temperatures above 250 °C, all four polymers showed significant weight loss due to the decomposition of the PPV main chains.

Polymer **P1** has a glass transition $T_g \sim 30$ °C which is presumably due to the motion of the polymer (PPV) chains. For polymers **1d**, **2d**, and **3d**, each exhibits two glass transitions; one characterized by a low T_g in the range between −45 and −65 °C, and a second glass transition with a T_g around 28 °C (see Figures 2e−g and Table 2). Since pure ethylene glycol has a glass transition temperature of about −75 °C (23), we relate the low glass transition of polymers **1d−3d** ($T_g \sim -45$ to −65 °C) to the presence of EG side chains. The second glass transition of polymers

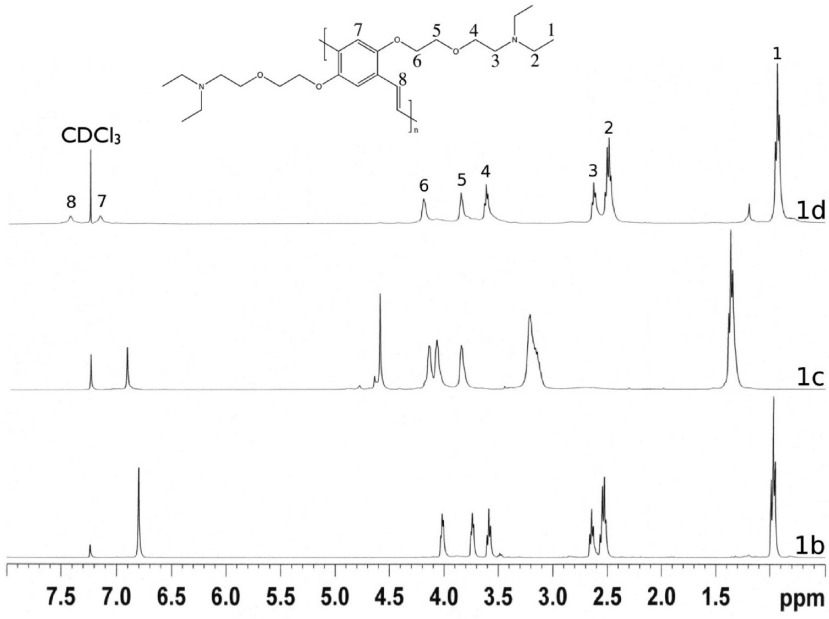

FIGURE 1. NMR spectra of polymer 1d and its precursors.

Table 1. Solubility of P1 and 1d−3d in Different Solvents[a]

Cmp	H_2O	MeOH	THF	EA	DCM	toluene
P1	0	0	<0.1	0	1	<0.1
1d	<0.1	1	3	<1	3	1
2d	3	5	5	10	10	5
3d	>10	5	5	10	5	3

[a] unit mg/mL, < 0.1 indicates a color change in solution but the amount of polymer dissolved is almost negligible.

1d−3d has a T_g value next to the glass transition temperature of polymer **P1** and relates to polymer (PPV) chain motion.

Microstructure. The presence of two distinct glass transitions in a single polymer is a rather unique observation for systems such as those described here, as these phenomena are typically observed for phase separated systems, e.g., block copolymers which self-assemble into separated hydrophobic and hydrophilic domains. The two-glass transition behavior can be readily observed in the difference in the microstructure adopted by these novel polymers when casted from hydrophobic and hydrophilic solvents. Figure 3 shows atomic force microscopy topographic images of polymer **3d** casted from aqueous solution (Figures 3a,b) and from dichloromethane (DCM, Figures 3c,d), both on silicon substrates. When casted from an aqueous solution, polymer **3d** forms large (∼500 nm size) micelle-like structures presumably with the polymer backbone as internal hydrophobic domain and EG side chains as the external hydrophilic domain (see cartoon depicting a proposed model in Figure 3b). When the same polymer is casted from dichloromethane, it forms inversed micelle-like structures which are significantly smaller (∼100−200 nm size) and presumably with the EG side chains now forming the internal hydrophilic domain (see cartoon depicting a proposed model in Figure 3d).

Crystallinity. Processability and the optical properties of the as-synthesized conjugated polymers are largely dominated by how polymer chains pack together to form structures of various orders. The XRD spectra of these as-synthesized polymers are taken in their original powder form and are shown in Figure 4b. Polymer **P1** is semicrystalline, with the XRD spectrum displaying multiple and sharp peaks representing several distinct *d*-spacings between polymer chains. The first peak at 5.1 degrees corresponds to a *d*-spacing of 14.6 Å (long-range order between polymer chains), a value consistent with the calculated value (14.3 Å) in the assumption that polymer side chains are extended with a slight overlap between diethylamines (see Figure 4a). Polymer **1d** has a liquid crystalline-like scattering pattern with a sharp peak at 4.68 degrees and an amorphous halo at approximately 23 degrees. A value of 4.68 degrees corresponds to a *d*-spacing between two polymer chains of 19.6 Å which is consistent with the calculated value of 20.14 Å, as estimated from the presumed structure shown in Figure 4a. It is reasonable to assume that the longer side chain of polymer **1d** is not as stiff as the shorter side chain of polymer **P1**, leading to a collapse of chain packing at short *d*-spacings, thus resulting in the liquid crystalline-like XRD patterns. Polymers **2d** and **3d** have similar diffraction patterns with a single amorphous halo center around 20 degrees (see Figure 4b). The *d*-spacings for these polymers are 3.64 Å (**2d**) and 3.66 Å (**3d**), and they are the result of $\pi-\pi$ stacking between polymer chains. The very small difference in $\pi-\pi$ stacking from polymer **2d** to polymer **3d** may be attributed to the interaction between side chains of various lengths.

The synthetic approach reported here demonstrates control over polymer crystallinity by varying the length of the side chains which in turn influences how polymer chains pack in order to form hierarchical three-dimensional structures. These as-synthesized conjugated polymers evolve

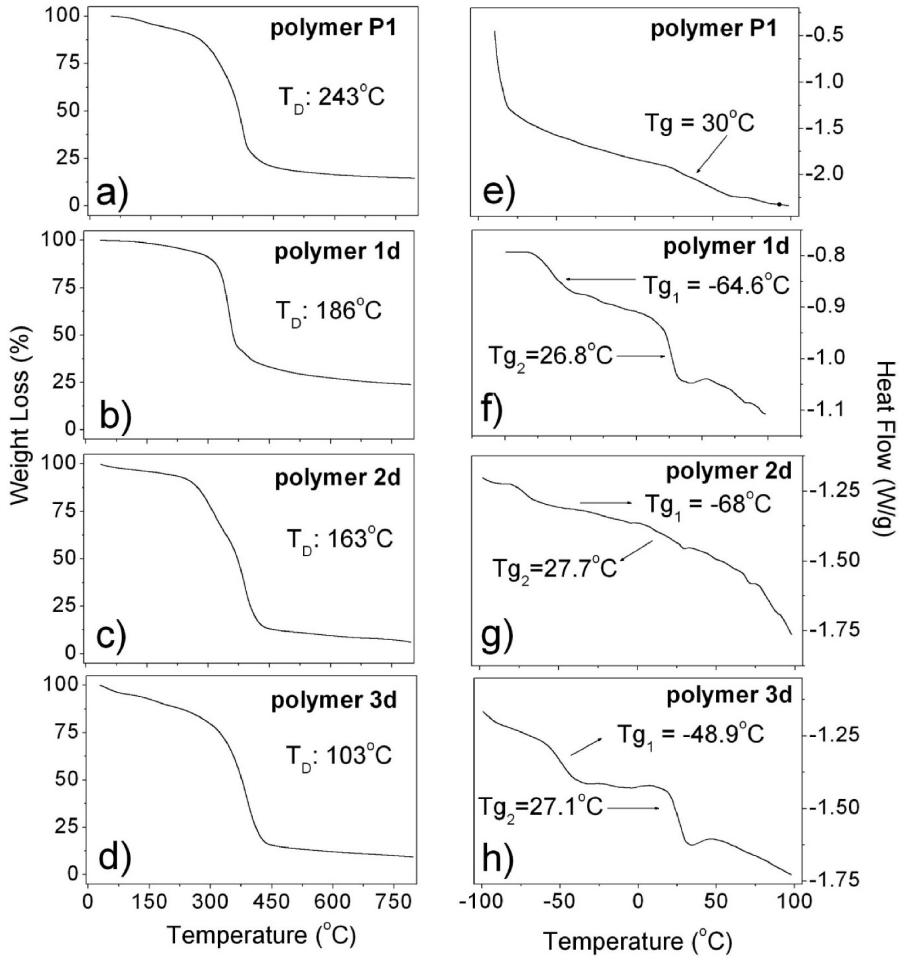

FIGURE 2. (a–d) Thermo gravimetric analysis (TGA) and (e–h) differential scanning calorimetry (DSC) of polymers P1, 1d, 2d, and 3d.

Table 2. Physical Properties of Polymers P1, 1d, 2d, and 3d

Cmp	M_W (10^3)	T_D (°C)	T_g (°C)	E_{ox} (V)	E_{red} (V)	EA	λ_{max}^{abs} (nm)	λ_{max}^{PL} (nm)	QY	τ_1 (ns)	τ_2 (ns)
P1	10.7	243	30.0	0.78	−0.29	1.07	472	556	0.24	1.39 (17%)	0.50 (83%)
1d	15.8	186	−64.6, 26.8	1.06	−0.66	1.72	473	550	0.33	1.14 (10%)	0.49 (90%)
2d	35.9	163	−68.0, 27.7	1.30	−0.61	1.91	451	539	0.31	1.22 (17%)	0.50 (83%)
3d	32.5	103	−48.9, 27.1	1.43	−0.38	1.81	463	545	0.28	1.38 (20%)	0.64 (80%)

[a] Physico-chemical parameters were estimated for polymers dissolved in dichloromethane. Quantum yields were estimated against rhodamine 110 in water. M_w: weight average molecular weight; T_D: decomposition temperature; T_g: glass transition temperature; E_{ox}: oxidation potential; E_{red}: reduction potential; EA: estimated band bap energy; λ_{max}^{abs}: peak absorption wavelength; λ_{max}^{PL}: peak emission wavelength; QY: photoluminescence (corresponding contributions given in parenthesis) quantum efficiency; $\tau_{1,2}$: photoluminescence lifetime.

from semicrystalline to liquid crystalline-like and finally to completely amorphous structure by simply increasing the length of the side chain. Longer EG side chains inhibit packing of polymer chains with long-range order, mainly because of the softness of the ethylene glycol.

Chain packing can be further impacted by temperature. Figure 5 displays temperature-dependent XRD spectra of polymer **1d**. As the temperature increases, the low angle XRD peak shifts to the right with a concomitant decrease in intensity, indicating a decrease in the overall order as well as a decrease in the long-range spacing between polymer chains. This result suggests that, as we heat the polymer **1d** to 65 °C, a temperature well below the decomposition temperature and slightly above the T_g, *d*-spacing dominated by the PPV main chain becomes shorter, presumably due to the collapse of the side chains at higher temperatures.

Electrochemical Properties. Cyclic voltammograms (CVs) for polymers **P1**, **1d**, **2d**, and **3d** measured in dichloromethane in the −1.7 to +2.4 V range (vs Ag/AgCl) are shown in Figure 6. The CVs were measured in solution rather than in film (e.g., by coating a polymer thin film on the electrode surface) to allow for direct comparison with UV–vis spectroscopy data measured in the same solvent (see below). The band gap energy of polymers is estimated from the difference between peak potentials of the first set of redox couple. Polymer **P1** exhibits a single redox couple and lacks a second oxidation peak (see Figure 6a). For polymers **1d**, **2d**, and **3d**, the addition of EG side chains changes the electronic structure in two ways. First, a second redox peak becomes clear for these EG substituted polymers (Figure 6b–d). Second, a monotonic increase in the band gap

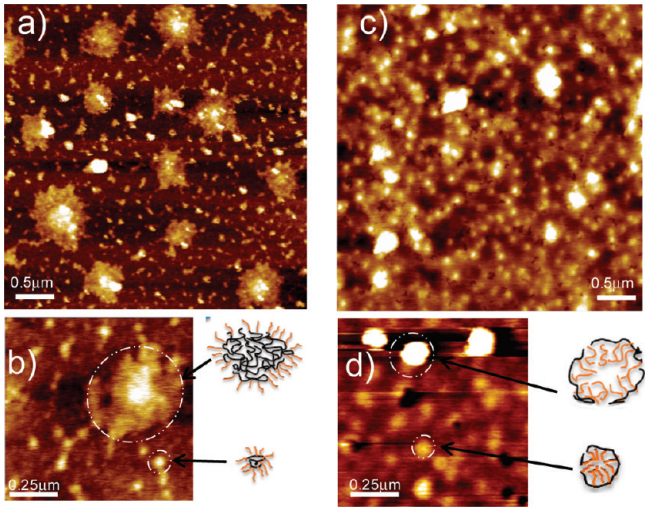

FIGURE 3. Atomic force microscopy images of polymer 3d casted from water (a, b) and dichloromethane (c, d) on a silicon substrate. Polymer 3d casted from aqueous solution forms large (~500 nm size) micelle-like structures with polymer backbone as internal hydrophobic domain and ethylene glycol side chains as external hydrophilic domain, as depicted in the cartoon shown in panel b). When polymer 3d is casted from dihloromethane on a silicon substrate, it forms small (~100−200 nm size) inverse micelle-like structures with the ethylene glycol side chains forming the internal hydrophilic domain, as depicted in the cartoon shown in panel d).

energy occurs when compared to the corresponding band of **P1** (1.07 eV, see Table 2), with the band gap energy increasing in this order: **2d** (1.91 eV) > **3d** (1.81 eV) > **1d** (1.72 eV). This observation is consistent with the UV−vis spectra of these polymers in dichloromethane (see Table 2) for which a similar trend is observed. However, some differences exist between the calculated bandgap energy from CVs and the values of the absorption peaks (λ_{max}^{abs}, see Table 2), e.g., data differ by 0.2−0.3 eV. One reason for this difference might be related to the fact that the CV measurements are carried out in solution; a situation where redox reactions lead to charge transfer species which are readily solvated, thus showing irreversible electrochemical response. On the other hand, the position of the redox peaks of the CVs is highly dependent on the scan rate, solvent, and polyelectrolyte. We also notice an inconsistency between the band gap energy of **P1** estimated from the UV−vis spectrum and from the redox potentials, mainly because we can only measure the first set of redox couple from which the band gap energy is being determined. Repeated experiments confirm this inconsistency, and we attribute this inconsistency to the low solubility of **P1** in dichloromethane due to the highly crystalline nature of this polymer.

It is noteworthy that all EG substituted polymers exhibit two reduction and two oxidation peaks, suggesting the injection of two charges/electrons into the polymers (see Figures 6b−d). Our results show not only the possibility of stabilizing two electrons by longer EG side chains but also the formation of structural domains, which can then potentially be developed into phase separated bulk heterojunctions for photovoltaic devices.

Photophysical Properties. The photophysics of the as-synthesized polymers was investigated in dichloromethane, a "good" solvent for all four polymers, as indicated by DLS which showed no evidence of aggregate formation. By excluding the presence of polymer aggregates, changes in the optical properties can be related to conformational differences resulting from the side-chain-dependent polymer−solvent interaction.

Polymer **P1** exhibits photophysics similar to PPV, with a broad visible absorption band peaking at 473 nm, a characteristic of the $\pi-\pi^*$ transitions originating from the phenylene vinylene conjugated backbone (11, 24). The photoluminescence (PL) spectrum of **P1** is vibronically structured with a main peak at 556 nm and a shoulder at ~610 nm. The PL quantum yield of **P1** in DCM is around 24%. The time-resolved PL decay of **P1** is biexponential, with lifetimes of 1.4 ns (17% contribution) and 0.5 ns (83%) (see Figure 7 and Table 2). The PL quantum yield is defined by $Q_{PL} = k_r/(k_r + k_{nr}) = \tau/\tau_r$, where k_r and k_{nr} represent the rate constants for radiative and nonradiative deactivation, respectively, and $\tau = 1/(k_r + k_{nr})$ and $\tau_r = 1/k_r$ are the measured lifetime and the radiative (natural) lifetime, respectively. For a biexponential time-dependent PL decay profile, the PL quantum yield can be written as $Q_{PL} = \alpha_1\tau_1/\tau_r + \alpha_2\tau_2/\tau_r$, with $\alpha_{1,2}$ weighted contributions of the measured lifetimes $\tau_{1,2}$ (26). Based on the values listed in Table 2, the estimated radiative lifetime for **P1** is ~2.5 ns. There is a visible difference between the shapes of the absorption and PL spectra of **P1** in dichloromethane, with the latter resembling more the spectrum of a single emitting species (see Figure 7a). We also noticed a large Stokes' shift between the two spectra (~83 nm). One possible reason for this difference in shape is an inhomogeneous broadening of the absorption spectrum due to disorder in the electronic delocalization, similar to that proposed by Friend and co-workers for PPV (26). Assuming a polymer chain is a composition of many conjugated segments of various lengths, separated by defects in the polymer chain (e.g., defects introduced by chain coiling), optical excitation with light of sufficient energy can excite all segments in a polymer chain, leading to exciton energy migration from shorter segments to longer sequences which have lower energy. While the absorption spectrum will be a sum of segments of many conjugation lengths, the PL will be due primarily to the longer sequences. In this assumption, some of the longer segments in **P1** exhibit long lifetimes (~1.4 ns), and they account for unquenched PL. However, most of the longer segments acting as energy traps are quenched, as suggested by the large contribution of the short lifetime (~0.5 ns, 83%) and by the relatively low PL quantum yield of **P1**.

The absorption and PL spectra of the ethoxy-substituted polymers dissolved in dichloromethane are all spectrally blue-shifted compared to **P1** (see Figure 7 and Table 2). The hypsochromic shift increases in the following order: **2d** > **3d** > **1d**. One would assume the blue shift will follow a trend similar to that of hydrophilicity, **3d** > **2d** > **1d**. This peculiar difference is likely due to a minimized polymer−solvent interaction for polymer **3d** in micellar domains, which renders polymer **3d** less coiled than polymer **2d**. It is

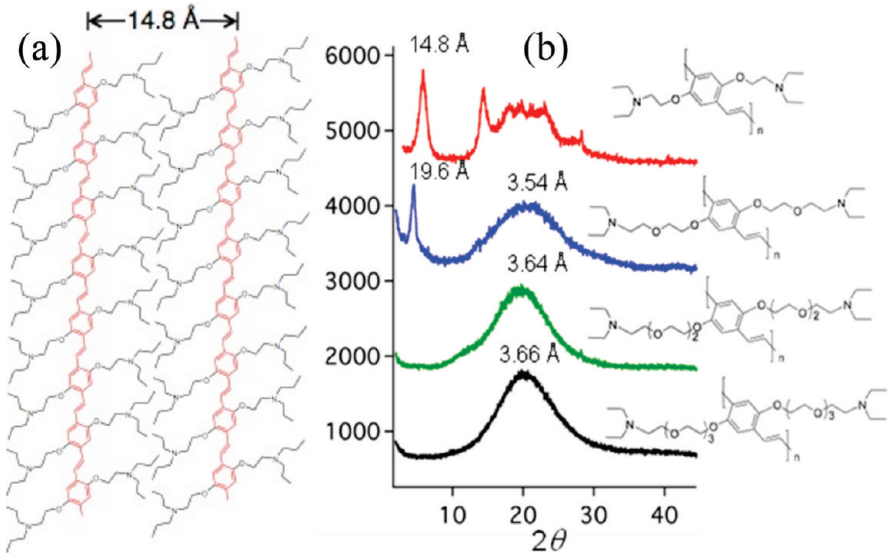

FIGURE 4. (a). Model depicting the packing of polymers P1 (semicrystalline) and 1d (liquid crystalline-like) as suggested by XRD. (b) XRD spectra of polymers P1, 1d, 2d, and 3d (top to bottom).

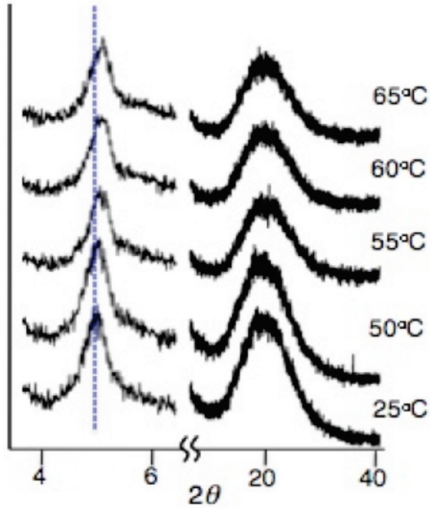

FIGURE 5. Temperature-dependent XRD spectroscopy of polymer 1d.

noteworthy that both the PL and the absorption spectra of the EG-substituted polymers show different shapes when compared to the corresponding spectra of polymer **P1**. The PL spectra of the EG-substituted polymers show loss of vibrational structure (Figure 7b–d), with the vibronic shoulder at longer wavelength becoming less prominent in the following order (see Figure 7e, circles, ratio of intensities of the first (main) and second vibronic peaks): **2d** > **3d** >**1d** > **P1**. Similarly, there is a broadening of the visible absorption bands of these polymers compared to polymer **P1**, in the following order (see Figure 7a–d and Figure 7e, triangles): **2d** > **3d** > **1d** > **P1**. This suggests an increased conformational flexibility for the conjugation system responsible for the visible absorption and emission (here the PPV main chain), an effect that we attribute to the presence of the EG repeat units. The time-dependent profile of the EG-substituted polymers is similar to that of **P1** (see Figure 7f), with a biexponential profile consisting of a long (~1.1 to 1.4 ns) and a short (~0.5 to 0.6 ns) lifetime (see Table 2). The

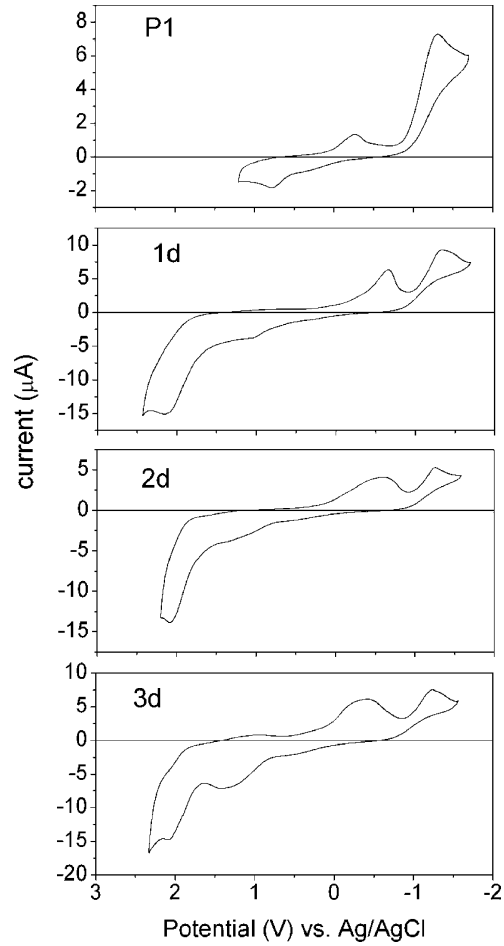

FIGURE 6. Cyclic voltammograms of polymers P1, 1d, 2d, and 3d in dichloromethane (vs Ag/AgCl). Polymer concentration ~10^{-3} M; *n*Bu4NPF6 as electrolyte.

estimated radiative lifetimes for these polymers are 1.72 ns (**1d**), 2.1 ns (**2d**), and 2.2 ns (**3d**).

Polymer **3d** exhibits good water solubility. From DCM to water, the main peaks of the absorption and PL spectra shift slightly toward blue, from 463 to 443 nm and from 545 to

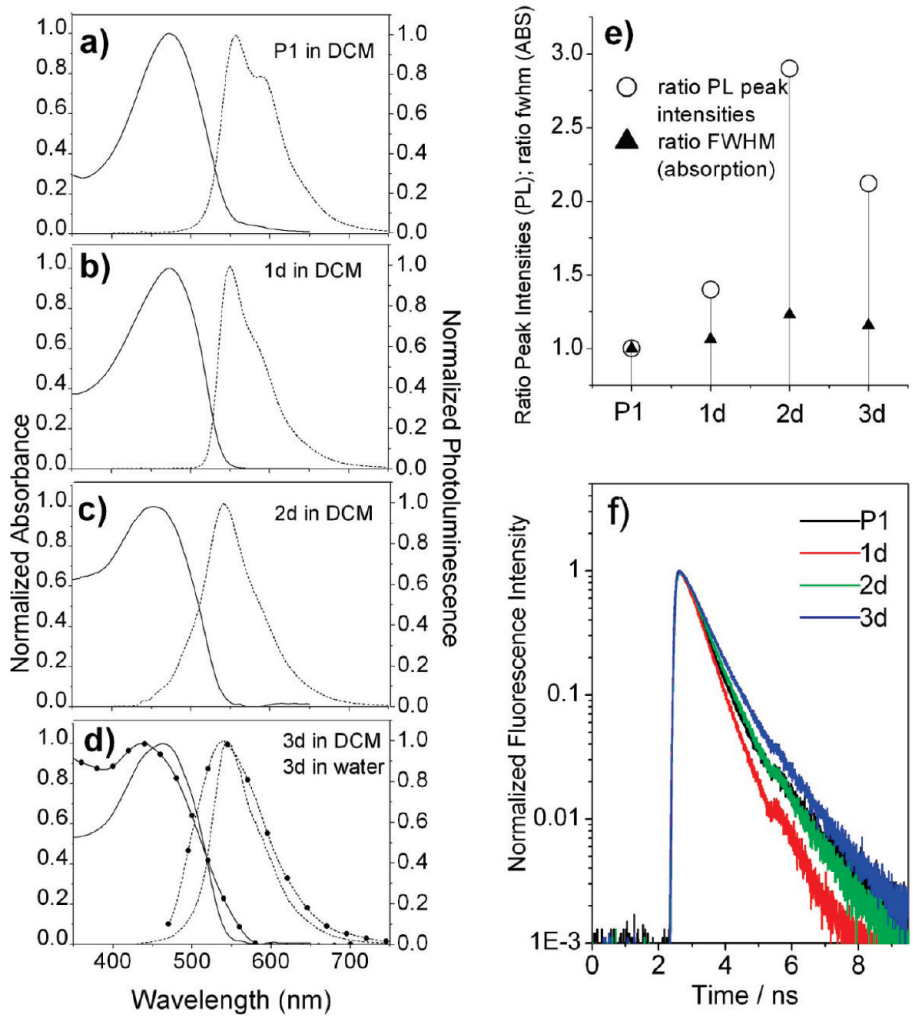

FIGURE 7. (a–d) Normalized absorption (solid line) and photoluminescence (dash line) spectra of polymers P1 and 1d–3d in dichloromethane. (d) Line and dots are absorption and PL spectra of polymer 3d in water. (e) Ratio of PL intensities corresponding to the main and second vibrational peak (circles) for polymers P1 and 1d–3d and ratio of the full width at half-maximum of the visible absorption band of polymers 1d–3d to the corresponding one of polymer P1 (triangles). (f) Photoluminescence decays of polymers P1 and 1d–3d in dichloromethane (see text for experimental details).

537 nm, respectively (see Figure 6d), suggesting a decrease in the conjugation length which usually refers to a less extended polymer chain conformation. There is also considerable broadening of both the absorption and PL spectra in water for polymer **3d**. In particular, the PL spectrum shows broadening at both blue and red spectral sides, features that are usually related to formation of aggregates due to the strong coupling of chromophores, as they are brought together via inter- and intrachain interactions. The presence of such aggregates explains the relatively low quantum yield of PL of polymer **3d** in water, around 0.12. Dynamic light scattering confirms the presence of small aggregates of sizes of ~80 nm. Considering the highly hydrophilic nature of the polymer side chain and hydrophobic nature of the main chain, polymer **3d** may adopt a micellar-like structure in water with a PPV core and EG (hydrophilic) shell, as shown in Scheme 2 and demonstrated here by atomic force microscopy (see Figure 3) and dynamic light scattering.

Scheme 2. Proposed Model for the Conformational Structure Adopted by Polymer 3d in Polar (Water) and Organic (Dichloromethane) Solvents[a]

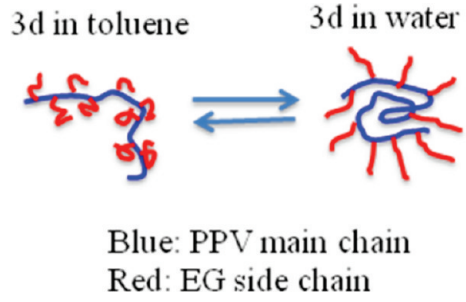

[a] The PPV main chain and ethylene glycol side chain are depicted in blue and red, respectively.

CONCLUSIONS

We have reported the synthesis of a series of fluorescent, conjugated polymers via the Gilch reaction with an overall yield greater than 40%. The increased EG repeat units on polymer side chains render solubility in water and concomitantly lead to a side-chain-dependent conformation and

solvent-dependent photophysics. Meanwhile, increasing the length of flexible polymer side chain leads to changes in chain packing; hence, the crystallinity evolves from semicrystalline to liquid crystalline-like to completely amorphous. These novel polymers exhibit two glass transition temperatures, which can be observed by differences in microstructure when casted from hydrophobic and hydrophilic solvents. These novel EG substituted polymers exhibit two reduction and two oxidation peaks in their CVs, suggesting the possibility of stabilizing two electrons by the use of ethylene oxide side chains. The potential of having a nanoscaled domain structure and stabilizing two electrons on a polymer chain signifies the potential of these polymers in fabricating electronic and photovoltaic devices.

Acknowledgment. This research was supported by the U.S. Department of Energy, Office of Basic Energy Sciences, Division of Materials Science and Engineering. Research was also carried out in part at the Center for Functional Nanomaterials, Brookhaven National Laboratory, which is supported by the U.S. Department of Energy, Division of Materials Sciences and Division of Chemical Sciences, under Contract No. DE-AC02-98CH10886 (MC, ZX with user HLW). Research was also performed, in part, at the Center for Integrated Nanotechnologies, a U.S. Department of Energy, Office of Basic Energy Sciences user facility at Los Alamos National Laboratory (Contract DE-AC52-06NA25396) and Sandia National Laboratories (Contract DE-AC04-94AL85000) (DW, with user HLW). We thank Dr. Kumara Mudalige from Brookhaven National Laboratory in Upton, New York, for help with atomic force microscopy and dynamic light scattering experiments.

Supporting Information Available: MALDI-TOF mass spectra of all polymer precursors: compounds 1b, 1c, 2b, 2c, 2d, 3a, 3b, and 3c. This material is available free of charge via the Internet at http://pubs.acs.org.

REFERENCES AND NOTES

(1) Ferreira, M.; Rubner, M. F. *Macromolecules* **1995**, *28*, 7107–7114.
(2) Fou, A. C.; Onitsuka, O.; Ferreira, M.; Rubner, M. F.; Hsieh, B. R. *J. Appl. Phys.* **1996**, *79*, 7501–7509.
(3) Baur, J. W.; Kim, S.; Balanda, P. B.; Reynolds, J. R.; Rubner, M. F. *Adv. Mater.* **1998**, *10*, 1452–1455.
(4) Garnier, F.; Korri-Youssoufi, H.; Srivastava, P.; Mandrand, B.; Delair, T. *Synth. Met.* **1999**, *100*, 89–94.
(5) Faid, K.; Leclerc, M. *Chem. Commun.* **1996**, 2761–2762.
(6) Gaylord, B. S.; Heeger, A. J.; Bazan, G. C. *Proc. Natl. Acad. Sci. U.S.A.* **2002**, *99*, 10954–10957.
(7) Gaylord, B. S.; Heeger, A. J.; Bazan, G. C. *J. Am. Chem. Soc.* **2003**, *125*, 896–900.
(8) Pinto, M. R.; Schanze, K. S. *Synthesis-Stuttgart* **2002**, 1293–1309.
(9) McQuade, D. T.; Pullen, A. E.; Swager, T. M. *Chem. Rev.* **2000**, *100*, 2537–2574.
(10) Zhao, X.; Jiang, H.; Schanze, K. S. *Macromolecules* **2008**, *41*, 3422–3428.
(11) Gao, Y.; Wang, C. C.; Wang, L.; Wang, H. L. *Langmuir* **2007**, *23*, 7760–7767.
(12) Xue, C. H.; Donuru, V. R. R.; Liu, H. Y. *Macromolecules* **2006**, *39*, 5747–5752.
(13) Bianchi, C.; Grassl, B.; Francois, B.; Dagron-Lartigau, C. *J. Polym. Sci., Part A: Polym. Chem.* **2005**, *43*, 4337–50.
(14) Wang, H. Q.; Duan, L.; Qiu, Y.; Wang, X. G.; Liu, D. S. *J. Appl. Polym. Sci.* **2002**, *83*, 2195–2200.
(15) Cacialli, F.; Friend, R. H.; Feast, W. J.; Lovenich, P. W. *Chem. Commun.* **2001**, 1778–1779.
(16) Morgado, J.; Cacialli, F.; Friend, R. H.; Chuah, B. S.; Rost, H.; Holmes, A. B. *Macromolecules* **2001**, *34*, 3094–3099.
(17) Zou, Y. P.; Tan, S. T.; Yuan, Z. L.; Yu, Z. J. *J. Mater. Sci.* **2005**, *40*, 3569–3571.
(18) Sumranjit, J.; Lahti, P. M. *Polymer* **2007**, *48*, 5514–5519.
(19) Winkler, B.; Dai, L. M.; Mau, A. W. H. *Chem. Mater.* **1999**, *11*, 704–711.
(20) Tasch, S.; Holzer, L.; Wenzl, F. P.; Gao, J.; Winkler, B.; Dai, L.; Mau, A. W. H.; Sotgiu, R.; Sampietro, M.; Scherf, U.; Mullen, K.; Heeger, A. J.; Leising, G. *Synth. Met.* **1999**, *102*, 1046–1049.
(21) Cotlet, M.; Goodwin, P. M.; Waldo, G. S.; Werner, J. H. *ChemPhysChem* **2006**, *7*, 250–260.
(22) Anelli, P. L.; Ashton, P. R.; Ballardini, R.; Balzani, V.; Delgado, M.; Gandolfi, M. T.; Goodnow, T. T.; Kaifer, A. E.; Philp, D.; Pietraszkiewicz, M.; Prodi, L.; Reddington, M. V.; Slawin, A. M. Z.; Spencer, N.; Stoddart, J. F.; Vicent, C.; Williams, D. J. *J. Am. Chem. Soc.* **1992**, *114*, 193–218.
(23) Shen, Z. Q.; Simon, G. P.; Cheng, Y. B. *Eur. Polym. J.* **2003**, *39*, 1917–1924.
(24) Johari, G. P. *Polymer* **1986**, *27*, 866–870.
(25) Shi, S. Q.; Wudl, F. *Macromolecules* **1990**, *23*, 2119–2124.
(26) Samuel, I. D. W.; Crystall, B.; Rumbles, G.; Burn, P. L.; Holmes, A. B.; Friend, R. H. *Chem. Phys. Lett.* **1993**, *213*, 472–478.

AM900766S